

# Surface modified and controlled $\text{CF}_x$ cathode material for ultrafast discharge and high energy density

Yang Dai<sup>1+</sup>, Sendan Cai<sup>1+</sup>, Lijun Wu<sup>3</sup>, Weijing Yang<sup>1</sup>, Jingying Xie<sup>1,5\*</sup>, Wen Wen<sup>4</sup>, Yi Zheng<sup>1</sup>, Jin-Cheng Zheng<sup>2\*</sup>, and Yimei Zhu<sup>3\*</sup>

<sup>1</sup>Shanghai Institute of Space Power Sources, Shanghai 200245, China

<sup>2</sup>Department of Physics, and Fujian Provincial Key Laboratory of Theoretical and Computational Chemistry, Xiamen University, Xiamen 361005, China

<sup>3</sup>Condensed Matter Physics & Materials Science Department, Brookhaven National Laboratory, Upton, New York 11973, United States

<sup>4</sup>BL14B1 Shanghai Synchrotron Radiation Facility, Shanghai, 201204, China

<sup>5</sup>Shanghai Engineering Center for Power and Energy Storage Systems, Shanghai 200245, China

+ Yang Dai and Sendan Cai contributed equally to this work

\* Correspondence and requests for materials should be addressed to J. X. ( [Jyxie@mail.sim](mailto:Jyxie@mail.sim.ac.cn).

ac.cn), J. Z. ( [jczheng@xmu.edu.cn](mailto:jczheng@xmu.edu.cn)) and Y. Z. ( [zhu@bnl.gov](mailto:zhu@bnl.gov))

**Keywords:** primary lithium batteries; carbon fluoride; de-fluorination; ultrafast discharge

$\text{Li}/\text{CF}_x$  primary possesses the highest energy density of 2180Wh/kg among all primary lithium batteries. However, a key limitation for its utility of this type of batteries is its poor rate capability because the cathode material,  $\text{CF}_x$ , is intrinsically a poor electronic conductor. Here, we report on our development on a controlled process of surface de-fluorination under mild hydrothermal condition to modify the highly fluorinated  $\text{CF}_x$ . The modified  $\text{CF}_x$ , consisting of an in-situ generated shell

component of F-graphene layers, possesses good electronic conductivity and removes the transporting barrier for lithium ions, yielding a high-capacity performance and excellent rate-capability. Indeed, a capacity of 500 mAh/g and a maximum power density of 44800 W/kg can be realized at ultrafast rate of 30 C (24A/g), that is over one-order-of-magnitude higher than that of the state-of-the-art primary lithium-ion batteries.

The Li/CF<sub>x</sub> primary battery is the first lithium battery developed since 1970's, and possesses the highest energy-density among all primary lithium batteries (theoretically 2180Wh/kg). In critical environment, such as deep underground or those far afield, in tire-pressure monitoring systems, and in space exploration, the cutting-edge CF<sub>x</sub> chemical system offers a long service-life, high reliability, a wide range of operating temperature and demonstrated excellent electrochemical performances that is not achievable by the common lithium- or so-called beyond lithium-systems (such as lithium-sulfur batteries, lithium-air batteries, sodium-sulfur batteries, and so on) systems. However, the Li/CF<sub>x</sub> battery is known to suffer from kinetic problems due to the intrinsically poor electronic conductivity of the cathode material CF<sub>x</sub>, inhibiting its applications in high-power devices<sup>1-4</sup>. Considerable efforts have been devoted to addressing these problems. Various nanoscale carbon materials, such as carbon nano-fibers<sup>5</sup>, carbon nanotubes, fullerenes<sup>4</sup>, and ordered meso-porous carbon<sup>6</sup>, were fluorinated by various methods to improve their electrochemical performances. An impressive 8057 W/kg power density (6C)

associated with a capacity of 440 mAh/g was achieved in fluorinated carbon fibers<sup>5</sup>. Other approaches were devoted to modifying the CF<sub>x</sub> materials. Generally, researchers usually applied the “doing addition” methods to achieve the modification, such as polypyrrole coating<sup>3</sup>, carbon-thermal treatment<sup>7, 14</sup>, and grapheme/SVO ball milling<sup>2</sup>. However, the rate capability remained limited. And the CF<sub>x</sub> reported in literature so far failed to realize a discharge rate over 10 C. Unfortunately, the CF<sub>x</sub> cathode also exhibits a low capacity at high rates (termed “low Faradic yield” ), so compromising the energy density. Thus, the challenge is on how to design and prepare the CF<sub>x</sub> material that possesses high rate capability without trading off energy density.

In this paper, we report an alternative “doing subtraction” approach to modify highly fluorinated CF<sub>x</sub>. We realize it by applying a controlled surface de-fluorination process under mild hydrothermal conditions. During defluorination, an electrical conductive surface is generated and the barriers to ion transport are removed. Once the limitation on electron transfer and ion transport at the electrode level are removed, the innate rate capability of CF<sub>x</sub> is revealed to be very high. We demonstrated that, even the CF<sub>x</sub> can also achieve an ultrahigh power-density of 48800W/kg at 30C, with a capacity of 500 mAh/g. The electrochemical performances, especially the rate capability are significantly improved compared to those of the state-of-the-art.

## Results

**Material synthesis and structural characteristics.** Although highly fluorinated CF<sub>x</sub> is hard to de-fluorinate at low temperature (<300 °C), it is still easy to react with NaOH in an H<sub>2</sub>O/CH<sub>3</sub>CH<sub>2</sub>OH solution, even at a lower temperature (180 °C) under

hydrothermal conditions. In this study,  $\text{CH}_3\text{CH}_2\text{OH}$  played a paramount role, serving as the co-solvent and the “surfactant” to wet the  $\text{CF}_x$  powder. From the optical photograph (leftmost part of **Figure 1**), the color of the pristine material is light gray, indicating the precursor graphite has been highly fluorinated. During the hydrothermal process (rightmost part of Figure 1), the C-F bond on the surface of the pristine  $\text{CF}_x$  is activated to form a new shell, leaving F in the solution. Thus, the color of modified  $\text{CF}_x$  turns shiny black, with F content decreasing from 62 to 58.7 wt%. This reduction of surface F content also affects the contrast quality of the SEM images. Figure 1 shows the typical layer stacking structure and the morphology of pristine  $\text{CF}_x$  with a particle size of about several to twenty micrometers, indicating the  $\text{CF}_x$  is generated from the graphite precursor. The blurred edges of the pristine particles point to their poor conductivity. In comparison, the SEM image of the modified one is clear, revealing the superior electron conductivity after hydrothermal treatment. In addition, the morphology of the modified particle exhibits more cracks, shaped like those in weathered granite. This might be induced by being “struck” by alkali ions under the high temperature and pressure conditions. The synchrotron x-ray diffraction pattern ( **Figure S2**) of the pristine  $\text{CF}_x$  shows typical broad peaks corresponding to the fluorinated phases (radiation wave length: 0.124nm), with  $2\theta \approx 10^\circ$  ,  $20.4^\circ$  and  $32.6^\circ$  assigned, respectively, to the  $\text{CF}_x$  (002) ( referred as  $\text{P}_1$  below), graphite (002) (referred as  $\text{P}_2$ ) and graphite (100) (referred as  $\text{P}_3$ ) peaks. It appears that the position and shape of the diffraction peaks do not change after the modification, implying that the de-fluorination process does not affect the major

structure of the particles<sup>3</sup>. However, a close inspection, especially a quantitative fitting of the peaks, reveals that the intensities ratio of the P2/P1 and P3/P1 increase from 0.11 to 0.17, xxx to xxx after modification, indicating an increase in graphite structure.

To understand how the structure changes after modification, we carried out structural analysis using high resolution transmission electron microscopy (HRTEM). Figure 2 shows the HRTEM images taken from pristine  $\text{CF}_x$  (Figure 2a), and modified  $\text{CF}_x$  particles (Figure 2b, 2c). The pristine  $\text{CF}_x$  presents irregular atomic arrangement, which is common in highly fluorinated graphite<sup>8</sup>. Inside the particle, e.g. in the bottom of (a) and (b), the modified  $\text{CF}_x$  has basically the same amorphous structure as the pristine  $\text{CF}_x$ . However, on the surface, e.g. top part of (a) and (b), the modified  $\text{CF}_x$  presents fringes like graphite or diamond polytypes<sup>15,16</sup>, while the pristine  $\text{CF}_x$  still exhibits an irregular atomic arrangement. These results indicate the graphite and diamond polytypes are the major structure on the surface region (up to several tens of nanometers) in the modified  $\text{CF}_x$ . To further confirm the structural changes on the surface of the modified  $\text{CF}_x$ , we carried out EELS spectrum image analysis in scanning transmission electron microscopy (STEM) mode in our double aberration corrected microscope (for details, see Fig. S1). Figure 2d shows the composition of C and F as a function of distance from the surface for pristine and modified  $\text{CF}_x$  calculated from the EELS spectrum image in Fig. S1. While the compositions of C and F are constant for pristine  $\text{CF}_x$ , the F concentration decreases from the interior of the particle to the surface. In the surface region ( $\sim 15$  nm), the concentration of F

drops considerably. The results clearly show that the surface of the modified  $\text{CF}_x$  particle is de-fluorinated and also the rearrangement of the F-graphene layers ( $\text{sp}^2$  or  $\text{sp}^3$  carbon rearrangement), while the core is basically unchanged, echoing the overall decrease of  $\text{CF}_x$  structure (or the increase of graphite) revealed by XRD. Raman spectra of different  $\text{CF}_x$  are depicted in **Figure S3**; a pair of peaks is observed around  $1340\text{ cm}^{-1}$  (D-band) and  $1580\text{ cm}^{-1}$  (G-band). The intensity ratio of the D and G bands ( $I_D/I_G$ ), is known to depend on the number of defects within the  $\text{CF}_x$  (the disorder-induced band). The  $I_D/I_G$  ratio of pristine  $\text{CF}_x$  is 1.39, thus confirming the presence of C-F  $\text{sp}^3$  hybridized carbon atoms <sup>[9]</sup>. On the other hand, the defect ratio for the modified  $\text{CF}_x$  ( $I_D/I_G = 1.85$ ) is higher, indicating the increase in defect concentration after de-fluorination. As will be discussed later, the superior electrochemical performance of modified  $\text{CF}_x$  can be attributed to the advantageous features offered by its unique microstructure.

The surface structure change can be further analyzed by surface-sensitive X-ray photoelectron spectroscopy (XPS). From the F1s XPS spectrum in **Figure 3a**, a characteristic peak is found at 689.8 eV in pristine  $\text{CF}_x$  corresponding to the covalent F species that exists in highly fluorinated carbon <sup>[1]</sup>. In comparison, a small shift about 1.0 eV is evident in Figure 3b, revealing a change in the chemical environment for F atoms after de-fluorination. The F 1s peak in semi-ionic and ionic C-F bonds are located at 688.2 eV and 685.9 eV respectively, <sup>[6]</sup> from which we speculate that after modification, parts of the covalent C-F bonds are transformed into semi-ionic ones,

which is reasonable for lower F content moieties (C/F=1.5) (see detailed XPS peak fittings and assignments in **Figure S5** and **Table S1**). As shown in Figures 3c and d, the C1s of pristine and modified  $\text{CF}_x$ , two components of C-containing (284.6 eV for  $\text{C}=\underline{\text{C}}<$ ,  $\text{sp}^2$  hybridization) and the F-containing moieties ( $\text{sp}^3$  hybridization, associated with the  $-\text{CF}_2$  and  $-\text{CF}_3$  groups) are exhibited.<sup>8</sup> The normalized peak area ratio of F-containing and C-containing moieties for pristine  $\text{CF}_x$  is estimated at 2.47 while a dramatic decrease of about 2 is represented in the modified  $\text{CF}_x$ , i.e. 0.44. Moreover, the difference between the  $\text{sp}^3$  and  $\text{sp}^2$  hybridization peaks for pristine and modified  $\text{CF}_x$  reduced from 6.5eV to 4eV. which may be due to the formation of lower F content species, such as  $\text{C}-\text{C}(\text{CF}_3)_3$  (288.2 eV) and  $\text{FC}(\text{C})_3$  (289.2 eV) after de-fluorination.<sup>[6]</sup> In fact, for the highly fluorinated  $\text{CF}_x$ , high F content species such as  $\underline{\text{F}}\text{C}(\text{CF}_3)_2$  (located at 291.0 eV) and  $\text{F}_2\underline{\text{C}}(\text{CF}_2)_2$  (291.8 eV) groups are likely to be generated on the edge of sheets and at the defects in the precursor surface<sup>1,6</sup>. On the contrary, the bonding energy range for those high F content groups can hardly be found in modified  $\text{CF}_x$  (Figure 3d). In addition, compared to the pristine  $\text{CF}_x$ , the peak area ratio of C-containing to F-containing for modified  $\text{CF}_x$  is greatly enhanced (from 0.86 to 1.52). This increase could be attributed to the de-fluorination and rearrangement of the carbon atom to form  $\text{C}=\underline{\text{C}}<$  bonds during the hydrothermal process.

**Electrochemical performances.** Coin cells (2016) with a metallic Li counter electrode were used to evaluate the electrochemical performance of materials (**Figure 4a, b**). The pristine composite cathode delivers a discharge capacity of 825 mAh/g

(theoretical value 916 mAh/g,  $\text{CF}_{1.17}$ ) at 0.025 C, with a plateau of 2.5V. A voltage delay is obviously seen from the curve. Although using an optimized conducting network (VGCF 10 wt %) <sup>10</sup> and a stress relief current collector (carbon coated Al foil) <sup>11</sup>, the pristine  $\text{CF}_x$  still shows very poor electrochemical performance at the discharge rate of 2C, with a capacity of only 520 mAh/g. The modified  $\text{CF}_x$  cathode ( $x = 0.89$  estimated according to the F content of 58.7wt%) exerts a capacity of 820 mAh/g at 0.025C, close to the theoretical capacity (825 mAh/g). More interestingly, the discharge plateau rises to 2.65V without any voltage delay, verifying the good electronic and ionic conductivity of the active particles at the initial stage of discharge<sup>1-4</sup>. Whereas  $\text{CF}_x$  cathodes are known to suffer from sluggish kinetics, our modified  $\text{CF}_x$  electrodes demonstrated outstanding high rate capability. The specific capacity of the modified  $\text{CF}_x$  composite cathodes at the fast discharge rates of 5C and 20C is 757 and 715 mAh/g, respectively, which is impressively 92 % and 87 % of that at 0.025 C. Even at the ultrafast rate of 30 C (24 A/g), a significant high capacity of 500 mAh/g and a maximum power density of 44800 W/kg (based on the active material) still can be obtained. Clearly, despite of the large particle size (SEM images in Figure 2), lithium ions can still rapidly reach the inside of the active material. We also investigated the  $\text{CF}_x$  treated with different NaOH equivalents (0.36 g, and 2.88 g). Compared to the pristine samples, the rate performances were improved. The material treated with 0.72 g showed the best performance.

## Discussion

It is well known that the good electronic and ionic conduction is expected to

contribute to high capacity and high rate capability. During the high fluorination process of pristine  $\text{CF}_x$ , the  $-\text{CF}_2$  and  $-\text{CF}_3$ , which are considered as inactive groups hindering the lithium ion diffusion, are likely to be generated on the surface<sup>1</sup>. This would cause surface electronic insulation and ionic traffic blocking, leading to poor faradic yield and rate capability. In contrast, after de-fluorination, the surface inactive groups are eliminated, and rearrangements occur to form a more electronic conductive surface (see HREM results in Figure 2 and XPS results in Figure 3). The increase of electronic conductivity of  $\text{CF}_x$  after de-fluorination is supported by first principles all-electron calculations. As shown in Figure 6, the fully fluorinated  $\text{CF}_x$  with an  $x=1$  sheet presents wide-band-gap characteristics, while for de-fluorinated one such as  $\text{CF}_x$  with  $x=0.5$ , a metallic-like feature is observed. As shown in the schematic illustration (Figure 5), the conductive surface can lower the resistance for electron transfer and provide more electronic paths to form effective conducting-network in the electrode. More importantly, the traffic for ion transport is improved since surface inactive groups such as  $-\text{CF}_2$  and  $-\text{CF}_3$  have been removed during de-fluorination. As shown in previous reports on  $\text{CF}_x$  modification,<sup>[1-7]</sup> researchers devoted to the electron transfer, but overlooked the ion transport. Although the electronic conductivity is enhanced, the ion transport barriers (such as  $-\text{CF}_2$ ,  $-\text{CF}_3$ ), or ion transport paths disruption during the modification still exist. Thus, it was hard to achieve high rate capability ( $>10\text{C}$ ) and high faradic yield. In this study, graphite and diamond-like carbon domains formed in the outer layer provided abundant channels without any barriers for lithium-ion transport (Fig 2c)<sup>12, 13</sup>. Once the limitations are

removed, high capacity and ultrafast rate performances can be achieved. To better understand our findings, an analysis of electrochemical impedance spectrum (EIS) at the open circuit voltage (OCV) was performed (see Figure S6). Clearly, the the cell reaction resistance ( $R_c$ , the semicircles) of the modified  $CF_x$  are only about half that of the pristine one, revealing the low resistance and improved conductivity. The onset between the semicircle and the sloped line are indicative of reaction kinetics with higher frequencies representing faster reaction kinetics, which indicates primarily a low reaction resistance<sup>7</sup>. Therefore, the EIS measurements corroborated the effective promotion of electron and ion transfer by the modified  $CF_x$  electrode.

In conclusion, we have developed a simple and effective de-fluorination method to modify  $CF_x$  cathodes through a hydrothermal process. The modified  $CF_x$ , consisting of an in-situ generated shell component of F-graphene layers, possesses good electronic conductivity deprived of transporting barriers of  $-CF_2$ ,  $-CF_3$  groups for lithium ions. Thus, high capacity performance and excellent rate capability without capacity compromising can be obtained. A capacity of 500 mAh/g and a maximum power density of 44800 W/kg was realized at ultrafast rate of 30C (24A/g). Our findings demonstrate a new route to achieving high power density  $CF_x$  material. More importantly, the promising utilities for high-power, high energy and long service life using the modified  $CF_x$  material are exciting, particularly for application in launchers for space exploration and in life-saving medical devices.

## Methods

**Modification of  $CF_x$ .** Modified  $CF_x$  was synthesized by a simple hydrothermal reaction between precursor  $CF_x$  (Daikin corp. Graphite precursor,  $x=1.17$ ) and base water/ethanol mixed solution. In a typical procedure, an NaOH (0.72g) and  $CH_3CH_2OH$ /water mixture (90 mL, 50/50 wt %) was blended by ultrasonication for 1 min. Then, the mixture was transferred into a 150mL Teflon-lined autoclave and maintained at 180°C for 8 h. Afterwards, the autoclave was naturally cooled to room temperature, and the product was subsequently filtered through a microporous membrane and washed throughout with ultrapure water. Finally, the modified  $CF_x$  was obtained by vacuum drying at 60°C for 24 hours. If not special mentioned, the modified  $CF_x$  is assigned to be treated using this procedure. The C/F ratios of the  $CF_x$  were determined by a chemical method and carried out in Shanghai Institute of Organic Chemistry, Chinese Academy of Science (CAS).

**Material Characterization.** The surface morphologies of the  $CF_x$  were visualized by scanning electron microscopy (SEM) using a Hitachi S4800 microscope. HRTEM, atomically resolved scanning transmission electron microscopy (STEM) and electron energy loss spectroscopy (EELS) experiments were performed using the JEOL aberration-corrected transmission electron microscope (JEM-ARM200F) at Brookhavn National Laboratory. The microscope was equipped with a cold-field emission source and a Gatan Quantum ER energy filter. Under normal operating conditions, a probe size of 0.1 nm with a 0.5 eV energy resolution is routinely achieved. The structure of the samples was characterized by synchrotron radiation X-ray diffraction (XRD), using the BL14B1 beamline at the Shanghai Synchrotron

Radiation Facility (SSRF) and the wavelength of the X-ray employed is  $\lambda = 1.2398 \text{ \AA}$ . BL14B1 is a bending magnet beamline, and the storage ring energy of SSRF is 3.5 GeV. The beam was first collimated using a Rh/Si mirror and then monochromatized using a Si (111) double-crystal monochromator. After that, the beam was further focused by a Rh/Si mirror to the size of  $0.5 \text{ mm} \times 0.5 \text{ mm}$ . Higher-order harmonics were also rejected by the Rh/Si mirror. A NaI scintillation detector was used for data collection. X-ray photoelectron spectroscopy (XPS) was performed using a RBD upgraded PHI-5000C ESCA system (Perkin Elmer) with Mg  $K\alpha$  radiation ( $h\nu=1253.6 \text{ eV}$ ). A Shirley-type background was removed from the spectra before de-convolution.

**Electrode Fabrication.**  $\text{CF}_x$  (80 wt%) powder, PVDF resin (10 wt%, Kynar 761), and vapor grown carbon fiber (VGCF, 10%, Showa Denko Co.) were mixed and stirred vigorously in the presence of N-methyl-2-pyrrolidone to form a uniform slurry. The cathodes were prepared by spreading the same slurry onto carbon coated aluminum foil ( $18 \text{ }\mu\text{m}$ ) current collectors. The thickness of the composite active layers is set around  $25 \text{ }\mu\text{m}$  after drying and rolling depression. Then coated Al foil was punched into disks of 1.4 cm in diameter, of which, the active mass loading were about 2 mg. The theoretical capacity of the  $\text{CF}_x$  was calculated using  $Q = xF/[3.6(12+19x)]$  (where x is the fluorine content, F is the Faraday constant  $96.485\text{C/mol}$  and 3.6 is the conversion constant<sup>14</sup>).

#### **First principles calculations.**

First principles calculations were carried out using the WIEN2k code<sup>17</sup> with the method of full potential linearized augmented plane wave plus local orbital

(FP-LAPW+lo). The exchange-correlation interaction is described by the Perdew-Burke-Ernzerh of generalized gradient approximation (PBE-GGA)<sup>18</sup>. The muffin-tin radii are selected as 1.25 a.u. for C, and 1.30 a.u. for F. The k-points of 15x15x2 for Brillouin zone sampling are used in the calculations. The EELS images are obtained by TELNES2 package in the WIEN2k code.

### **Acknowledgement**

Financial support from the National Natural Science Foundation of China (No. 21103109, No.21373137, No.U1232110), and Shanghai Science and Technology Talent Program (No. 12XD1421900). No. ) are greatly appreciated. The specialized research fund for the doctoral program of higher education (No. 20100121120026). The work at Brookhaven National Laboratory is supported by the U.S. Department of Energy, Office of Basic Energy Sciences, under Contract No. DE-AC02-98CH10886.

### **Author contributions**

Y.Dai. and J. Xie conceived the idea. Y.Dai and S.Cai synthesized the materials and conducted the electrochemical tests. L.Wu. and Y. Zhu performed TEM/STEM/EELS characterizations. W.Yang and Y. Zheng performed the materials characterization and data analysis and W.Wen did the XRD experiments. J.C. Zheng organized the project, and performed first principles calculations. All the authors discussed the results and contributed to the manuscript.

### **Additional information**

Supplementary Information accompanies this paper at <http://www.nature.com/naturecommunications>

## References

1. Guerin, K., M. Dubois, A. Houdayer, A. Hamwi, Applicative performances of fluorinated carbons through fluorination routes: A review *J. Fluorine Chem.* **134**, 11-17 (2012).
2. P. Meduri, H. Chen, X. Chen, J. Xiao, M. Gross, T. Carlson, J. Zhang, Z. Deng, Hybrid CFX - Ag<sub>2</sub>V<sub>4</sub>O<sub>11</sub> as a high-energy, power density cathode for application in an underwater acoustic microtransmitter *Electrochem. Commun.* **13**,1344-1348 (2011).
3. H. Groult, C.M. Julien, A. Bahloul, S. Leclerc, E. Briot, A. Mauger. Improvements of the electrochemical features of graphite fluorides in primary lithium battery by electrodeposition of polypyrrole, *Electrochem. Commun.* **13**, 1074-1076 (2011).
4. M. Dubois, K. Guérina, W. Zhang, Y. Ahmad, A. Hamwi, Z. Fawal, H. Kharbache, F. Masin, Tuning the discharge potential of fluorinated carbon used as electrode in primary lithium battery. *Electrochimica Acta* **59**, 485-491, (2012).
5. P. Lam, R. Yazami, Physical characteristics and rate performance of (CF<sub>x</sub>)<sub>n</sub> (0.33 < x < 0.66) in lithium batteries, *J. Power Sources*, **153**, 354-359 (2006).
6. P. Fulvio, S. Brown, J. Adcock, R. Mayes, B. Guo, X. Sun, S. Mahurin, G. Veith, S. Dai, Low-Temperature Fluorination of Soft-Templated Mesoporous Carbons for a High-Power Lithium/Carbon Fluoride Battery, *Chem. Mater.* **23**, 4420-4427 (2011).
7. S. Zhang, D. Foster, J. Read, "Enhancement of discharge performance of Li/CF<sub>x</sub> cell by thermal treatment of CF<sub>x</sub> cathode material, *J. Power Sources* **188**, 601-

605 (2009).

8. Z. Wang, J. Wang, Z. Li, P. Gong, X. Liu, L. Zhang, J. Ren, H. Wang, S. Yang, Synthesis of fluorinated graphene with tunable degree of fluorination *Carbon* **50**, 5403-5410 (2012).

9. Y. Sato, M. Ootsubo, G. Yamamoto, G. Lier, M. Terrones, S. Hashiguchi, H. Kimura, A. Okubo, K. Motomiya, B. Jeyadevan, T. Hashida, K. Tohji, Super-Robust, Lightweight, Conducting Carbon Nanotube, *ACS nano* **2**, 348-356 (2008).

10. Y. Li, Y. Chen, W. Feng, F. Ding, X. Liu, The improved discharge performance of Li/CF<sub>x</sub> batteries by using multi-walled carbon nanotubes as conductive additive, *J. Power Sources* **196**, 2246-2250 (2011).

11. J. Read, E. Collins, B. Piekarski, S. Zhang, LiF Formation and Cathode Swelling in the Li/CF<sub>x</sub> Battery, *J. Electrochem. Soc.* **158**, A504-A510 (2011).

12. T. Brezesinski, J. Wang, S. Tolbert, Bruce Dunn, Ordered mesoporous  $\alpha$ -MoO<sub>3</sub> with iso-oriented nanocrystalline walls for thin-film pseudocapacitors *Nature materials* **9**, 146-151 (2011).

13. A. Magasinski, P. Dixon, B. Hertzberg, A. Kvit, J. Ayala G. Yushin, High-performance lithium-ion anodes using a hierarchical bottom-up approach, *Nature materials* **9**, 353-358 (2010).

14. Q. Zhang, S. D'Astorg, P. Xiao, X. Zhang, L. Lu Carbon-coated fluorinated graphite for high energy and high power densities primary lithium batteries, *J. Power Sources* **195**, 2914-2917 (2010).

15. P. Darrell Ownby, Yang, Xi, and Liu Jenq, Normal-Pressure Hot-Pressing of

Alpha-Alumina-Diamond Composites, *J. Am. Ceram. Soc.*, 75 [7] , 1876-1883 (1992);

16. K. E. Spear, Phelps, A. W., and White, W. B. Diamond polytypes and their vibrational spectra *J. Mater. Res.*, 5,(11) 2277-2285 (1990).

17. P. Blaha, K. Schwarz, G. K. H. Madsen, D. Kvasnicka, and J. Luitz, WIEN2k, An Augmented Plane Wave Plus Local Orbitals Program for Calculating Crystal Properties. Vienna University of Technology, Vienna, Austria, 2001.

18. J. P. Perdew, K. Burke, and M. Ernzerhof, "Generalized Gradient Approximation Made Simple," *Phys. Rev. Lett.*, 77, 3865–8 (1996)

**Figure 1** The optical micrographs and SEM images of the pristine and modified  $\text{CF}_x$  powders. Conductivity difference in the two materials is visible from the SEM images (the middle panel), as is blur for the pristine but much more clear for the modified one. The dark edge around the particles in the upper right part of the figure refers to the high F-containing moieties such as  $-\text{CF}_2$  or  $-\text{CF}_3$  groups in pristine  $\text{CF}_x$ . The light lines around the modified particles indicates the in-situ de-fluorinated layers, which possess a higher carbon content.

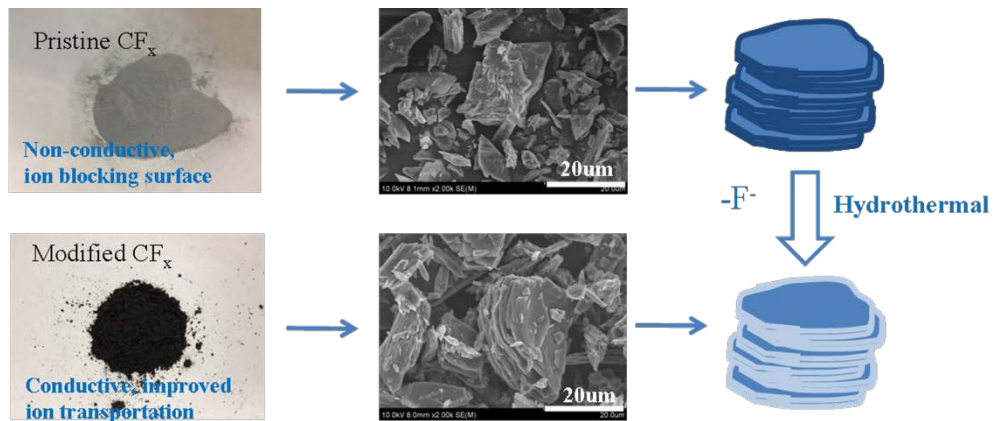


**Figure 2** (a-c) High resolution TEM (HRTEM) images taken from (a) pristine  $\text{CF}_x$ , and (b,c) modified  $\text{CF}_x$  particles. Inside the particle, i.e., in the bottom of (a) and (b), the modified  $\text{CF}_x$  has basically the same amorphous structure as the pristine  $\text{CF}_x$ . However, on the surface, i.e., top part of (a) and (b), the modified  $\text{CF}_x$  presents fringes like graphite or diamond polytypes, while the pristine  $\text{CF}_x$  still exhibits an irregular atomic arrangement. The spacing of the fringes in modified  $\text{CF}_x$  varies from 0.34 nm to 0.45 nm. The fringes shown in green and red box in (c) have the spacing of 0.35 nm and 0.41 nm, respectively, close to those of graphite and diamond polytypes, indicating the presence of graphite or diamond polytype structure on the surface region (up to several tens nanometers) in the modified  $\text{CF}_x$ . To further confirm the structure changes on the surface of the modified  $\text{CF}_x$ , we carried out EELS spectrum image analysis in scanning transmission electron microscopy mode in our double aberration corrected microscope (for details, see Fig. S1). (d) shows the C and F composition as a function of distance from the surface for pristine and modified  $\text{CF}_x$  calculated from the EELS spectrum image in Fig. S1. While the compositions of C and F are constant for pristine  $\text{CF}_x$ , the F concentration decreases from the interior of the particle to the surface. On the surface region ( $\sim 15$  nm), F concentration drops significantly.

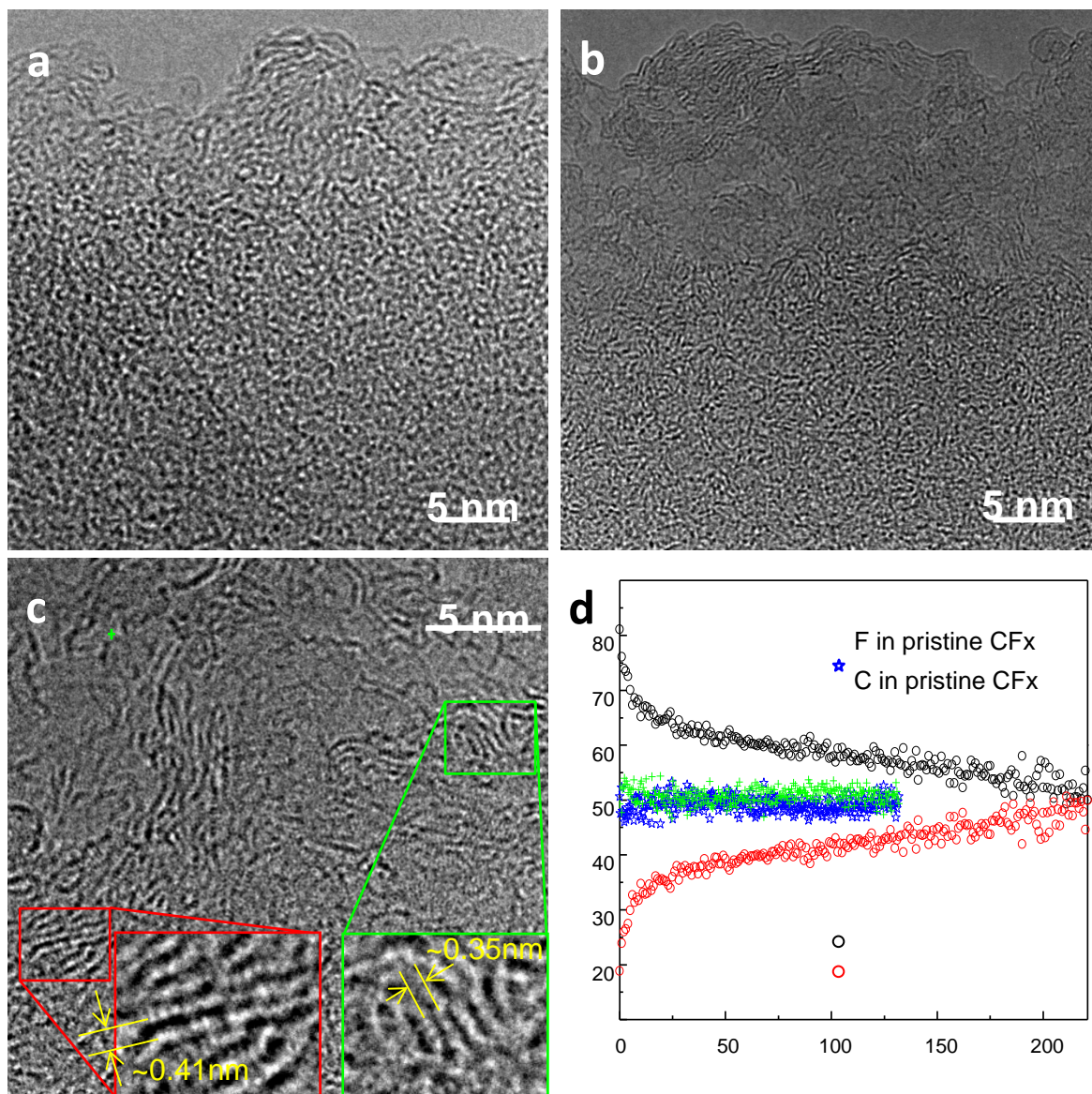


**Figure 3** X-ray photoelectron spectroscopy spectrum of F1s for (a) pristine and (b) modified  $\text{CF}_x$ ; and C1s for (c) pristine and (d) modified  $\text{CF}_x$ . (b) shows a small red shift of about 1.0 eV in comparison with (a). More importantly, distinct differences in peak area ratios and energy differences between  $\text{sp}^3$  and  $\text{sp}^2$  hybridized C1s for both materials can be identified in (c) and (d). Binding energy ranges from 291 eV to 293 eV for high F-containing groups such as  $\text{FC}(\text{CF}_3)_2$  (291.0 eV) while  $\text{F}_2\text{C}(\text{CF}_2)_2$  (292.5 eV) can hardly be found in (d) after modification.

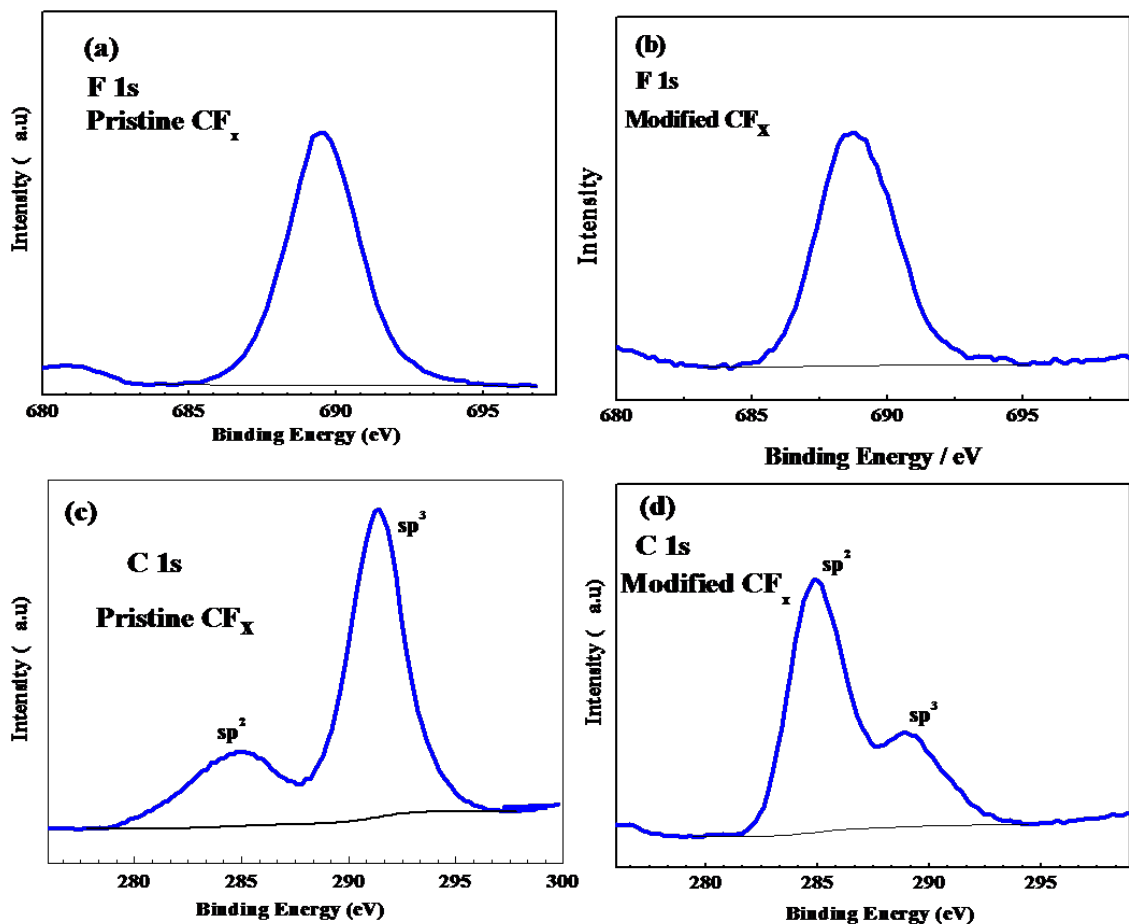


**Figure 4** Discharge profiles of (a) pristine and (b) modified  $\text{CF}_x$ . The voltage delay phenomenon is eliminated during the discharge process of the modified  $\text{CF}_x$  at the rate of 0.025C. The discharge curves in (b) show no significant capacity fade from 0.025C to 20C. Even a capacity of 500mAh/g can be delivered at the rate of 30C, and a maximum power density of 44800 W/kg (based on the active material) still can be obtained. However, the capacity that is exerted by the pristine  $\text{CF}_x$  at 2C is only 520 mAh/g.

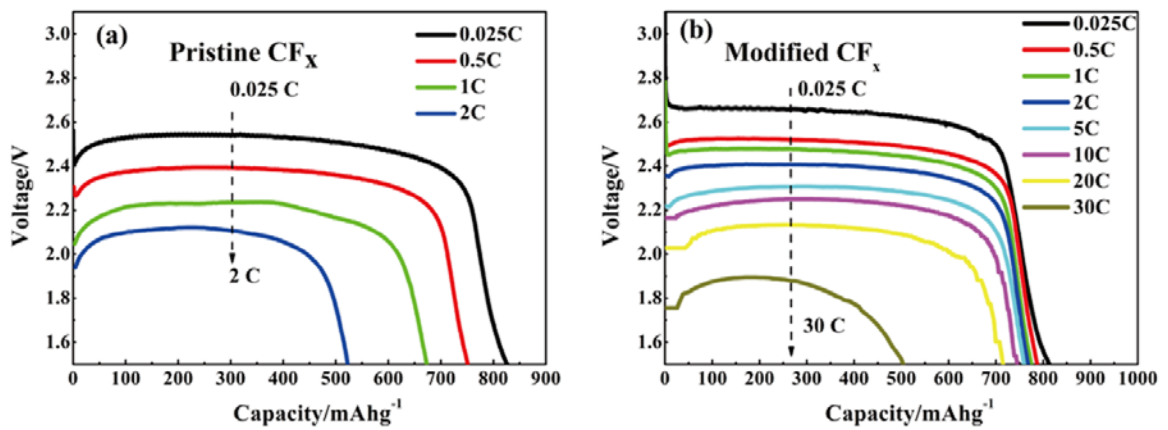


**Figure 5** Schematic diagram of electronic paths for pristine and modified CF<sub>x</sub> during discharge. The light edge around the particles in the left part of the figure refers to the high F-containing moieties such as -CF<sub>2</sub> or -CF<sub>3</sub> groups in pristine CF<sub>x</sub>. While the dark lines around the modified particles indicates the in-situ defluorinated layers, which possess a high carbon content. The conductive surfaces formed after hydrothermal treatment can lower the resistance and provide more paths for electron transfer, thus greatly improving the rate capability. Moreover, lower inner resistance means less heat generation.

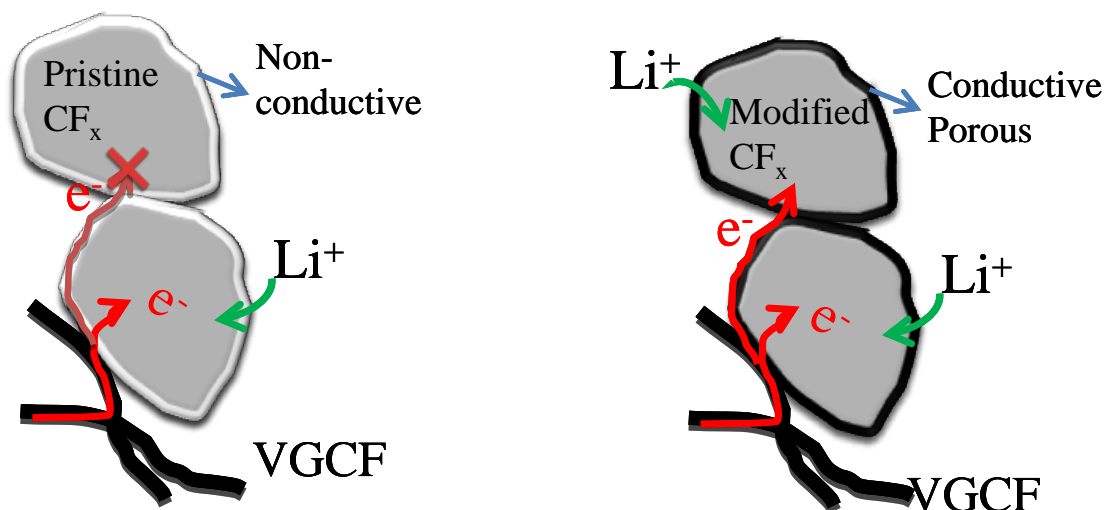
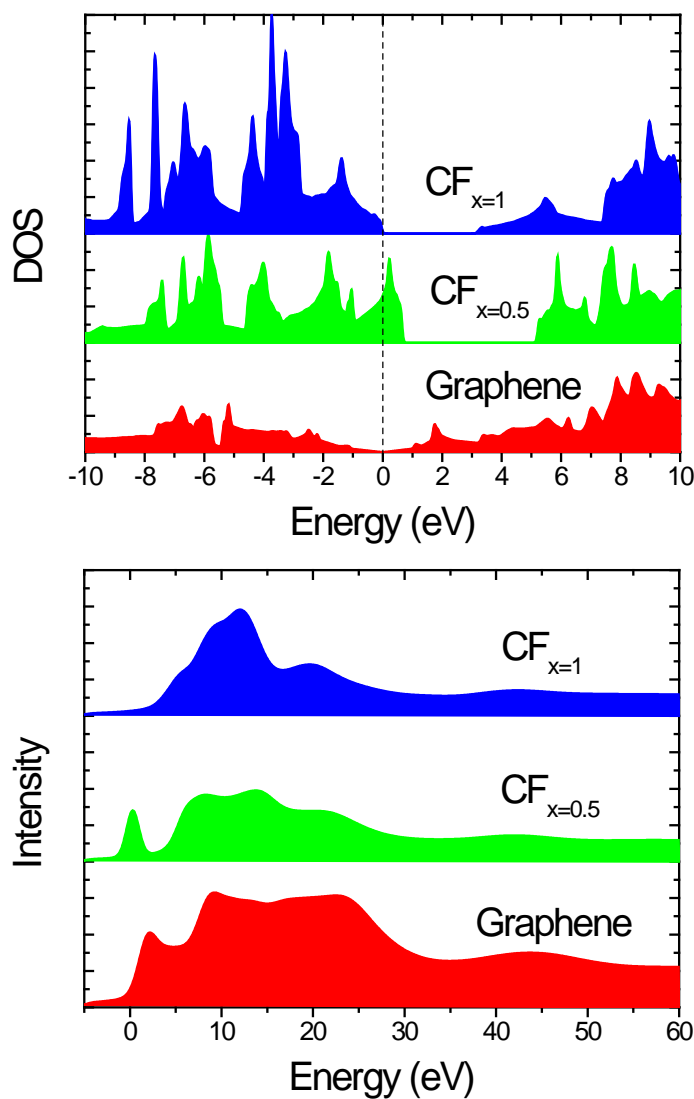


**Figure 6** Density of states (DOS) (a) and EELS (b) of CF<sub>x</sub> obtained by first principles all-electron calculations based on density functional theory. The Fermi energy is indicated by dashed line in (a). Fully fluorinated carbon, CF<sub>x</sub>(x=1), shows wide band gap. However, for CF<sub>x</sub> (x=0.5), it shows metallic like feature, as indicated by the high DOS at the Fermi level. The present of separated and significant prepeak in EELS (b) for CF<sub>x</sub> (x=0.5) comparing with CF<sub>x</sub>(x=1) is a signature of de-fluorination, which is in good agreement with experimental measurement (see Fig. S1).



## ToC

A simple and effective de-fluorination method is developed to modify  $\text{CF}_x$  cathodes through a hydrothermal process that greatly improves the capacity performance and rate capability of  $\text{CF}_x$  by removal of surface ionic transport barriers. A capacity of 500 mAh/g and a maximum power density of 44800 W/kg was achieved at an ultrafast rate of 30C (24A/g).

**Keywords:** primary lithium batteries; carbon fluoride; de-fluorination; ultrafast discharge

*Yang Dai, Sendan Cai, Lijun Wu, Weijing Yang, Yi Zheng, Jingying Xie\*, Wen Wen and Jin-Cheng Zheng\* Yimei Zhu\**

## $\text{CF}_x$ battery material for ultrafast discharge

ToC figure

